Weather and Climate Extremes 44 (2024) 100670

Contents lists available at ScienceDirect

Weather and Climate Extremes

journal homepage: www.elsevier.com/locate/wace

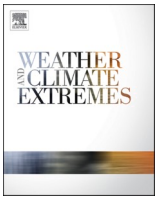

The role of soil moisture-temperature coupling for the 2018 Northern European heatwave in a subseasonal forecast

Sunlae Tak [a,1], Eunkyo Seo [b,c,1], Paul A. Dirmeyer [c], Myong-In Lee [a,*]

[a] Civil Urban Earth and Environmental Engineering, Ulsan National Institute of Science & Technology (UNIST), 50 UNIST-gil, Ulju-gun, Ulsan, 44919, Republic of Korea
[b] Department of Environmental Atmospheric Sciences, Pukyong National University, Busan, 48513, Republic of Korea
[c] Center for Ocean-Land-Atmosphere Studies, George Mason University, Fairfax, VA, 22030, United States

ARTICLE INFO

Keywords:
2018 Northern Europe heatwave
GloSea5
Land-atmosphere coupling processes
Breakpoint
Hypersensitivity

ABSTRACT

This study investigates the predictability of the 2018 Northern Europe heatwave using the GloSea5 forecast model from the perspective of land-atmosphere interactions. We focus on an inverse relationship wherein soil drying leads to increased temperatures and the model's ability to simulate this hypersensitivity in the soil moisture-temperature coupling on the dry side of a breakpoint defined as the soil moisture threshold below which land feedbacks nonlinearly amplify extreme heat. When evaluating forecast model performance in predicting this heatwave, we compare deterministic forecast scores (Hit Rate (HR) and True Skill Score (TSS)) for whether model Surface Soil Moisture (SSM) falls within the hypersensitive regime. GloSea5 exhibits enhanced prediction skill for the extreme heat event when the modelled soil moisture is within the hypersensitive regime. To understand the skill of the heatwave forecast for hit and missed cases of capturing SSM below the breakpoint, we first evaluate the climatological model performance for the water- and energy-limited processes, and then perform a comparison classified by whether SSM verifies on the dry side of the wilting point. The composite analysis demonstrates that the reproducibility of the breakpoint is tied to an improvement in climatological land coupling processes, mainly for classification in the water-limited coupling regime. Therefore, the results suggest that the process-based connection between soil moisture and temperature is a potential source for improving heatwave forecasts on subseasonal to seasonal (S2S) time scales.

1. Introduction

The occurrence of intensified heatwaves has been increasing under climate change. Climate extremes rarely occur independently but usually in combination, as droughts and heatwaves are concurrently characterized by high daily maximum temperatures accompanied by dry land surface conditions during the warm season (Kong et al., 2020; Miralles et al., 2012; Suarez et al., 2014). Land-atmosphere interactions can play an important role in exacerbating extreme heatwaves, where soil desiccation suppresses evaporation while enhancing sensible heat flux within the partitioning of surface energy under atmospheric high pressure (Miralles et al., 2014; Quesada et al., 2012; Seo et al., 2020).

Land surface processes are a major factor that characterize the coupling between soil moisture and land heat fluxes. Based on a critical value of soil moisture, two regimes of land-atmosphere interaction are categorized. The wet side of the critical point is an energy-limited regime in which the source energy at the land surface is mainly attributed to the atmosphere. In contrast, the dry side of the critical point of soil moisture is a water-limited regime where the partitioning of land fluxes between latent (LE) and sensible (H) heat flux is significantly controlled by the amount of soil moisture available to supply evaporation. The water-limited regime contains within it both a transitional and a dry regime. The transitional regime exhibits declining LE as soil moisture decreases, while the dry regime is typified by a nearly complete lack of evaporation. Soil moisture controls the surface energy partitioning in the water-limited regimes, and soil moisture is negatively correlated with the surface air temperature (Hirschi et al., 2010; Seneviratne et al., 2010). As dry soil moisture conditions tend to increase the allotment of absorbed radiative energy toward sensible heat flux, the land surface and near-surface air temperatures increase (Dirmeyer 2006). Positive temperature anomalies enhance evaporative demand and subsequently result in declining soil moisture. Such a positive

* Corresponding author.
E-mail address: milee@unist.ac.kr (M.-I. Lee).
[1] These authors contributed equally to this work.

https://doi.org/10.1016/j.wace.2024.100670
Received 6 November 2023; Received in revised form 19 February 2024; Accepted 3 April 2024
Available online 4 April 2024
2212-0947/© 2024 The Authors. Published by Elsevier B.V. This is an open access article under the CC BY license (http://creativecommons.org/licenses/by/4.0/).

feedback typically stresses the vegetation and influences surface albedo feedbacks that control radiative forcing. The energy exchange at the land surface alters the evolution of the boundary layer and further affects precipitation processes (Findell et al., 2011).

To understand the relevant land surface processes, many previous studies have suggested various diagnostic metrics using *in situ* observations, remote sensing, and modelling datasets. Santanello et al. (2018) illustrated a suite of local land–atmosphere coupling (LoCo) metrics at different spatial and temporal scales by statistical and process-based metrics. For instance, soil moisture memory is an autocovariance-based statistical metric to measure the persistence of daily soil moisture anomalies, which affects coupled feedback throughout the subseasonal time scale (Dirmeyer et al., 2016; Seo and Dirmeyer 2022a). Depending on the choice of source and target variables, segmented coupling processes can be measured as links in a chain of land and atmospheric feedbacks. There are several process-based coupling metrics to measure the land-atmosphere interactions where land states are not directly employed. They examine the process chain of land-atmosphere coupling within the diurnal cycle (Seo and Dirmeyer 2022b). Furthermore, to evaluate the representation of land coupling regimes in coupled forecast systems, water- and energy-limited processes are quantified to the temporal correlation coefficient of latent heat flux (the variable linking water and energy balances) with soil moisture and net radiation, respectively (Seo et al., 2024). The representation of observed land coupling regimes, relative balancing water- and energy-limited coupling, is crucial for model performances to simulate realistic atmospheric conditions relevant to land-atmosphere interactions.

For the fidelity of the relationship between the land surface wetness and near-surface air temperature, the sensitivity of temperature to soil moisture variability is strongest in dry conditions, which enables a key process in the development of heatwaves (Barriopedro et al., 2023; Seo et al., 2019). The breakpoint (BP) is a conceptual threshold value of soil moisture across which this sensitivity changes significantly. The dry side of the BP exhibits a stronger sensitivity of temperature to declining soil moisture due to the dominance of sensible heat flux in balancing land surface energy, compared with the wet side of the BP where evaporative cooling can offset other sources of heating (Benson and Dirmeyer 2021; Dirmeyer et al., 2021b). With the BP demarking a regime of temperature hypersensitivity in land-atmosphere coupling, Dirmeyer et al. (2021b) demonstrated the physical mechanisms of the development of 2018 Northern Europe heatwave using flux tower observations, finding the BP to be strongly associated with soil wilting point. The significant decrease in soil water content across large areas of Northern Europe triggered extraordinary land-atmosphere feedbacks, resulting in moisture limitations on LE, which in turn suppressed cloud formation and contributed to elevated temperatures during prolonged periods of extreme heat. Notably, most locations exhibited a critical threshold of soil water content, i.e., BP, below which evaporation, heating, and daily maximum temperatures demonstrate heightened sensitivity to declining soil moisture. Much of Northern Europe experienced an unprecedented state of dryness, emerging as a temporary "hot spot" for land-atmosphere coupling, intensifying the heatwave across a significant portion of the region.

Benson and Dirmeyer (2023) demonstrated the impact of the implementation of derived BP information on heatwave forecast skill in retrospective forecasts from S2S models over the contiguous United States but did not investigate the 2018 Northern Europe heatwave event nor the physical understanding of the improvement of extreme heat predictability corresponding to the model performance of land-atmosphere interactions. Only pre-existing model simulations were analysed (Pegion et al., 2019). This study aims to quantitatively confirm the fidelity of model simulated BP on the 2018 Northern Europe heatwave prediction using the Global Seasonal Forecast System version 5 (GloSea5) based on the evaluation of land-atmosphere coupling processes. The paper is organized as follows. Section 2 describes the GloSea5 model, and the validation datasets used in this study. Section 3 provides the methodology to define heatwave and evaluate the forecast performance. Section 4 presents and discusses the results of this study. Finally, Section 5 summarizes the results and their implications for future applications.

2. Data

2.1. Reanalysis data

The European Centre for Medium-Range Weather Forecasts (ECMWF) Reanalysis Version 5 (ERA5) is employed for validation in this study. It has a 25 km horizontal resolution (TL739) with hourly temporal resolution. A revised land surface Hydrology of the Tiled ECMWF Scheme for Surface Exchanges over Land (HTESSEL) land surface model is used to produce land surface outputs. ERA5 demonstrates superior performance in land surface variables, especially for soil moisture, when compared to several microwave soil moisture retrievals and reanalysis datasets (Beck et al., 2021). Compared with the previous ERA-interim, ERA5 boasts enhancements in its physical processes and incorporates over 240 parameters at the surface (Hersbach et al., 2020). It also utilizes advanced data assimilation systems for Integrated Forecast System (IFS) Cycle 41r2 4D-Var to improve data quality. It uses the observation operator from Radiative Transfer for Television infrared observation satellite Operational Vertical sounder (RTTOV)-11 for radiance data updated with the RTTOV-7 operator used in ERA-Interim. It also assimilates humidity-sensitive satellite channels using the all-sky approach instead of the clear-sky approach used in ERA-Interim. ERA5 integrates more satellite data, including all-sky information for various components and RTTOV-11 and observational near-surface data from stations over land, radiosondes, balloon and aircraft-based atmospheric observations. ERA5 assimilates precipitation data from ground-based radar observations. Soil moisture information is extracted from C-band microwave channels using reprocessed products based on the Advanced Scatterometer (ASCAT), European Remote-sensing Satellite (ERS)-1 and −2 (Hersbach et al., 2020). Daily 2-m maximum temperature (TMAX), top-layer (0–7 cm) soil water content (SSM), mean surface LE and H are used in this study. A 30-year (1989–2018) climatology period leading up to the study year is used in the daily time series of TMAX and SSM anomalies and the other analyses are carried out with a 6-year product (2016–2021). For the validation of model performance, ERA5 is upscaled to the forecast model resolution.

2.2. Forecast model

In this study, we use the fully coupled model component of the Met Office Global Seasonal Forecast version 5 (GloSea5)-GC2.0 system (MacLachlan et al., 2015) to quantify the role of land-atmosphere interactions on subseasonal heatwave prediction skill. The atmosphere and land surface components of the coupled model are the Global Atmosphere model version 6.0 (GA6.0) (Walters et al., 2017) and the Joint UK Land Environment Simulator (JULES) (Best et al., 2011), respectively. JULES is a tiled land surface model (LSM) representing sub-grid scale heterogeneity. The tile fractions are produced from 17 surface types in International Geosphere-Biosphere Programme (IGBP) mapped to the nine surface types in JULES (Loveland et al., 2000). There are five plant function types (broadleaf trees, needleleaf trees, C3 temperate grass, C4 tropical grass, and shrubs) and four non-vegetation types (urban, inland water, bare soil, and land-ice), in which surface parameters (e.g., albedo, roughness length) are defined for each specific land cover type. The surface energy balance for each tile encompasses fluxes of sensible heat and moisture, as well as latent heat of vaporization for snow-free tiles or sublimation for snow-covered or ice tiles. The heat flux into the ground, which combines radiative fluxes beneath vegetation canopies and conductive fluxes for the unvegetated fraction, is parameterized as a function of the thickness and temperature of the surface soil

layer. The JULES model's prognostic variables, such as soil moisture, are computed in response to atmospheric forcing variables. These variables include 2-m air temperature and humidity, precipitation, 10-m wind speed, radiative fluxes, and surface pressure (Best et al., 2011). The soil is divided into 4 vertical layers (the bottom of each layer is at 0.1, 0.25, 0.65, and 2 m below the surface).

The ocean component is the Nucleus for European Modelling of the Ocean (NEMO) (Mogensen et al., 2012), and the sea ice component is the Los Alamos sea ice model (CICE) (Rae et al., 2015). Semi-implicit semi-Lagrangian discretization is used to solve the fully compressible, non-hydrostatic atmospheric equations of motion in the dynamical core of the UM. The atmospheric model has a horizontal resolution of 0.56° latitude × 0.83° longitude. The initial atmospheric conditions for the forecast members are generated by the Korea Meteorological Administration (KMA) Global Data Assimilation and Prediction System (GDAPS) with N1280L70 resolution. The forecast soil moisture initial conditions are provided from the seasonally varying mean climatology of ERA-Interim without interannual variation, such that the forecast soil moisture is not initialized from the KMA data assimilation system. GloSea5 adopts the Forecast Ocean Assimilation Model (FOAM) Ocean Analysis in order to initialize the ocean components in the coupled model. The ocean and sea-ice initial conditions are taken from the short-range ocean forecasting and data assimilation system. The spread in ensemble initial conditions for each day (4 members per day) is generated using a stochastic physics scheme Stochastic Kinetic Energy Backscatter Scheme version 2 (SKEB2) (Bowler and Mylne 2009) providing small grid-level perturbations during the model integration. In this study, 30-day lead forecast datasets are validated throughout the 62 initiated forecasts during July and August 2018.

3. Methodology

3.1. Definition of a heatwave

This study defines an extreme heat day as any day that exceeds the 90th percentile for daily TMAX forecast with 4-member ensemble during a two-month summer season (July–August, JA) during 2016–2021. This threshold value is calculated for each forecast lead time and at each grid point. To ameliorate the model bias throughout the forecast lead time, different temperature thresholds are constructed. For the reanalysis data, the 90th percentile threshold value is obtained from daily TMAX of the JA period over 30 years (1989–2018) at each grid point.

3.2. Hypersensitivity regime

As soil moisture dryness leads to a decrease of LE based on limited water availability, the partitioning of net radiation (R_n) to H increases. This is a key process leading to increasing temperature through land-atmosphere interactions during the summer season. However, the response of TMAX to soil wetness reflects process nonlinearity such that the increase of TMAX corresponding to soil drying is accelerates in very arid conditions. In this situation, a hypersensitive response in the soil moisture-temperature relationship begins to appear. Surface soil conditions play a key role in developing, exacerbating, and possibly prolonging heatwaves. The BP value of SSM is defined to delineate the SSM value where a linear segmented regression of the temperature against the soil moisture on the dry side exhibits a negative slope that is significantly steeper than that on the wet side, while the two linear regressions are constrained to intersect at the same value of temperature at the BP (Benson and Dirmeyer 2021; Dirmeyer et al., 2021a).

To calculate the BP at each grid point, the error defined by the summation of the departure of samples against a pair of regression lines at both sides from the BP is minimized. In addition, stringent significance criteria are applied for the two estimated slopes by scaling the effective sample size of N days by the local soil moisture memory (time scale in days when the lagged autocorrelation drops below $1/e$) (Dirmeyer et al., 2016), to properly take into account the true degrees of freedom in the time series. Subsequently, p-scores are computed with a standardized error assumed to be a normal distribution in parameter estimates. A p-score of 0.01 or less is considered significant and retained for further analysis. Lastly, the slopes of the linear regressions on both sides of the BP should be negative and the slope on the drier side must be steeper than that on the wet side. The BP is calculated using TMAX and SSM variables in ERA5 reanalysis from July to August of during 2016–2021. The BP in the GloSea5 is calculated with 11–30 lead day forecast for each ensemble member initiated in July–August of 2018. The BP is calculated individually without taking into account the differences in surface layer depth between ERA5 and GloSea5. To elucidate the relationship between SSM and TMAX in the forecast model, we exclude the short-term up to 10-day lead forecasts, known to be significantly influenced by initial conditions.

3.3. Forecast verification methods

This study utilizes two deterministic forecast scores; Hit Rate (HR) and True Skill Score (TSS; also called the Hanssen and Kuipers discriminant). They are formulated as

$$HR = \frac{a}{a+c} \tag{1}$$

$$TSS = \frac{a}{a+c} - \frac{b}{b+d} \tag{2}$$

where variables *a, b, c*, and *d* are the number of cases of "Hit", "False alarm", "Miss", and "Correct rejection" in the contingency table (Table 1) (Hamill and Juras 2006), respectively. HR indicates the proportion of extreme events that the forecast model correctly catches. That is, HR represents the overall performance of the prediction model for capturing the occurrence of extreme heat or dry events, while TSS illustrates the model's ability in the prediction of extreme events considering that the model does not capture what does not appear in observations. In other words, TSS takes into account both correct and incorrect predictions of the forecast, and it is bounded from −1 to 1. The perfect forecast skill is 1, and 0 indicates that predictions are no better than random chance. TSS is less sensitive to event frequency and proves to be particularly useful when verifying forecasts with varying climatology (Tartaglione 2010). Furthermore, heatwave intensity is quantified using each ensemble member: only values exceeding the climatological 90th percentile threshold value ($TMAX_{90th}$) are chosen and then averaged for each lead time. Intensity is formulated as

$$Intensity = TMAX - TMAX_{90th} \tag{3}$$

In this study, two distinct contingency tables are employed: one for heatwave forecasting and the other for forecasting whether SSM is on the analysed side of the BP (the individually calculated soil moisture BP and $TMAX_{90th}$ from ERA5 and GloSea5 are used as threshold values for the deterministic decision in the first and second steps, respectively). Firstly, when hypersensitivity is detected in ERA5, the validation process includes confirming whether the modelled SSM value falls within the hypersensitive regime determined by the BP from GloSea5. This validation is carried out in both the ERA5 reanalysis and the forecast model at each grid point. Then, the heatwave cases are composited by the BP contingency table in the previous step and the forecast skill scores are calculated for each lead time. Based on the individually calculated

Table 1
2x2 Contingency table.

2X2 Contingency Table		Observation (reanalysis)	
		Yes	No
Forecast	Yes	Hit (a)	False alarm (b)
	No	Miss (c)	Correct rejection (d)

breakpoints in ERA5 and GloSea5, HR and TSS are compared to measure the heatwave predictability if the model simulates the hypersensitivity shown in the reanalysis.

3.4. Definition of water- and energy-limited regimes

This study assesses the representation of land coupling regimes in model simulation to understand key processes in land-atmosphere interactions based on the water and energy balance equations. The characteristic of land coupling, which is separated at the critical soil moisture value where the dry and wet sides experience water- and energy-limited conditions, respectively. Seo et al. (2024) classified the land coupling processes measured by the relative ratio of the temporal correlation coefficient of LE (a conjugate variable linking the water and energy cycles) with SSM and net radiation (key variables controlling water and energy balancing). This approach allows quantification of how land-atmosphere coupling is influenced by either the water- or energy-limited processes (see Fig. 5 in Seo et al., 2024). The model reality representing the land coupling regime is quantified by the 2-dimension spatial correlation coefficient, which takes into account horizontal pattern agreement, compared to the result of ERA5 reanalysis.

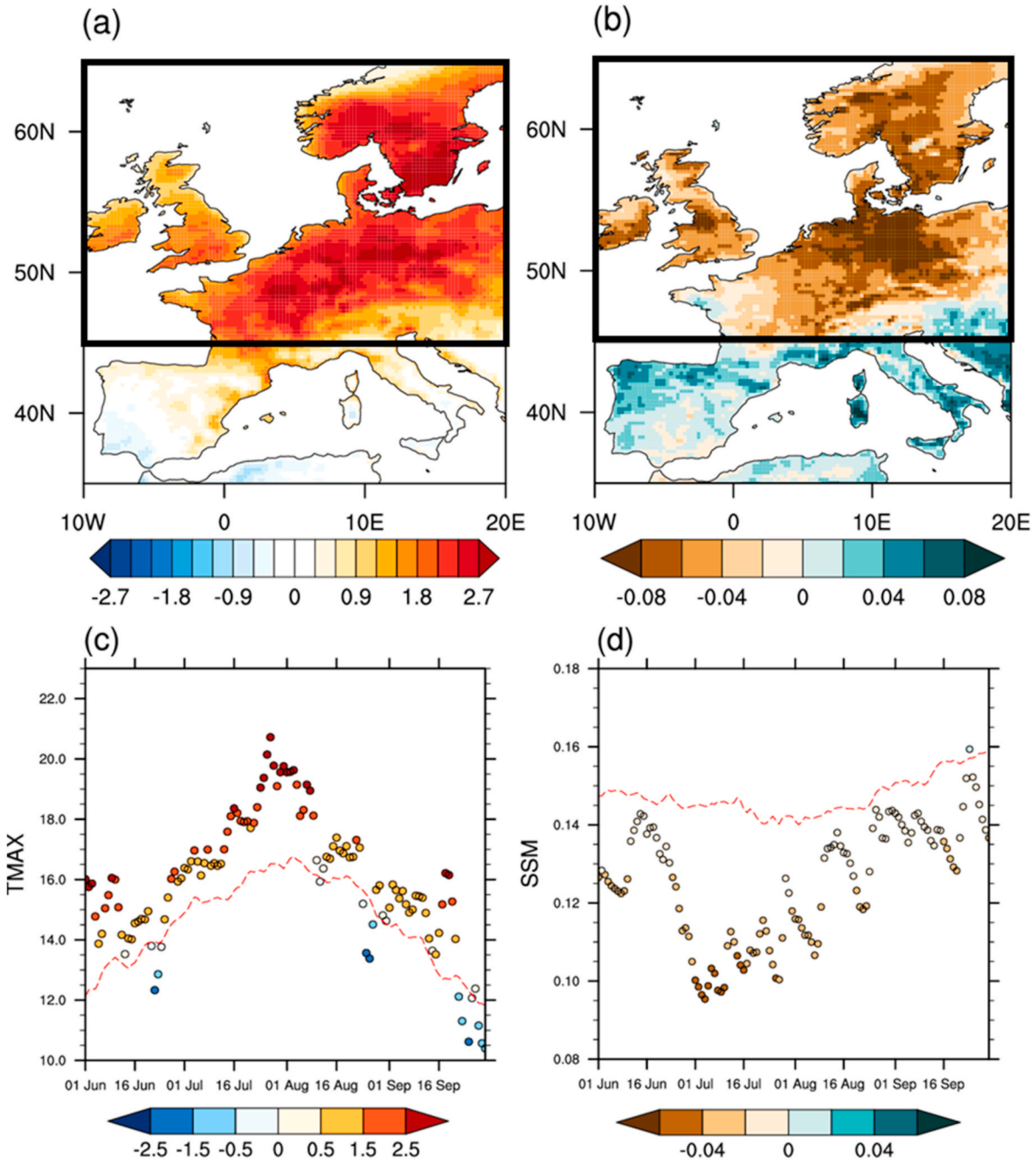

Fig. 1. The spatial distributions of (a) TMAX (units: K) and (b) SSM (units: m^3m^{-3}) anomalies during June to August (JJA) of 2018 over the Europe from ERA5 reanalysis compared with its 30-year (1989–2018) climatology. The daily time series of area averaged (c) TMAX and (d) SSM over Northern Europe (10°W–20°E, 45–65°N) in land grid points. Red lines and shaded dots indicate the daily climatology and anomaly for both variables. (For interpretation of the references to colour in this figure legend, the reader is referred to the Web version of this article.)

4. Results

For the 2018 summer season over the Europe, an extreme heatwave was accompanied by a drought event, mainly affecting southern Britain, southern Scandinavia, and the Northern European plain (Fig. 1a and b). Southern Sweden and Northern Germany, which lie at the core of the heatwave, exhibited a TMAX anomaly of 3.5 K during boreal summer season accompanied by anomalous dryness in soil water content. For instance, the daily time series of maximum temperature exhibits positive anomalies above 2.5 K from mid-July to early-August; the heatwave peaked with a temperature anomaly of 4 K during the end of July (Fig. 1c). The SSM anomaly over the Northern European plain was -0.07 m^3m^{-3}, which is 23 % below the climatological value (Fig. 1b). Correspondingly, daily SSM rapidly decreased due to the enhanced evaporation at the land surface in mid-June. During the heatwave peak period, the soil moisture anomaly was -0.04 m^3m^{-3} over Northern Europe and dryness persisted throughout the summer of 2018. The soil moisture deficit during the warm season amplifies the heatwave by allocating net radiation at the land surface mostly to the sensible heat flux. Additionally, the large gap between dew point temperature and actual temperature defines a higher lifted condensation level, which is an indicator of repressed cloud formation. It implies a decreased probability of precipitation accompanied by increasing downward shortwave radiation and a deepened planetary boundary layer (PBL). This is a favourable condition to entrain dry warm air from above the top of the PBL (Dirmeyer et al., 2021b). Other previous studies suggested that global warming significantly contributed to the development of the 2018 European heatwave (Leach et al., 2020; Wehrli et al., 2020) and the dry soil played an important role in its occurrence as land-atmosphere interactions aggravated the drought and the heatwave over the Northern European region (Dirmeyer et al., 2021b; Petch et al., 2020).

To understand the nonlinear relationship between soil water content and daily maximum temperature, particularly during the heatwave period, this study carries out a segmented regression analysis to identify the threshold BP value described in subsection 3.3. The relationship between SSM and TMAX generally shows a negative correlation in the water-limited region (Fig. 2a and e), indicating that dry soil contributes to higher maximum air temperatures. For instance, the defined BP threshold value over Central Europe (3.375E, 48.478N) in ERA5 is 0.198 m^3m^{-3}, and the slopes on the dry and wet side are -31.7 K/m^3m^{-3} and -5.1 K/m^3m^{-3} (Fig. 2a), respectively. The negative relationship is well captured by GloSea5 with 0.168 m^3m^{-3}, and the slopes on the dry and wet side are -11.2 K/m^3m^{-3} and -4.1 K/m^3m^{-3} (Fig. 2e), respectively. The BP from ERA5 and GloSea5 is calculated at each grid point. The spatial distribution of BP resembles the map of soil moisture climatology (not shown). The climatological BP in GloSea5 is not exactly same as the reanalysis due to sampling issues and the differences in spatial resolution. In addition, inconsistencies in some soil properties (e.g., wilting point) between both datasets contributes to the disagreement in values of BP. Central and Northern Britain and the Alps, which are climatologically wet areas, have BP defined with relatively high values (Fig. 2b). On the other hand, the Iberian Peninsula and the region around Poland exhibit low BP values. GloSea5 also represents a reliable spatial pattern of BP across the European region (Fig. 2f), where the pattern correlation with ERA5 is 0.94 over Northern Europe (10°W–20°E, 45–65°N). To avoid aforementioned inconsistency issues between ERA5 and GloSea5, when the BP value is rescaled to a percentile of climatological SSM for each product, it shows higher spatial agreement compared with the original pattern of the BP (not shown). This indicates that the model has the potential to simulate the observed heatwave response due to anomalous soil moisture conditions.

The ability of GloSea5 to simulate the TMAX increase with soil moisture decrease is estimated with the slope of a linear regression for

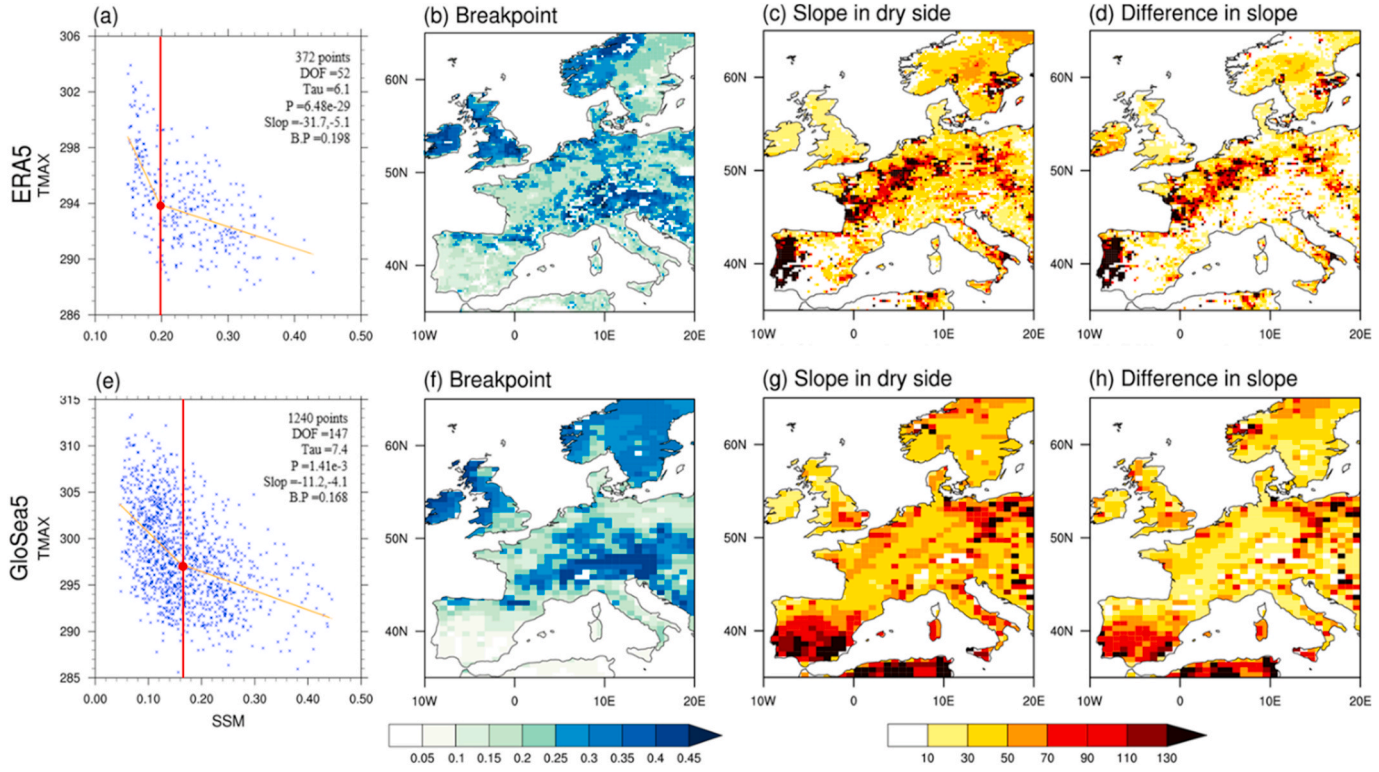

Fig. 2. (a) Scatter plot of daily TMAX (units: K) against volumetric SSM (units: m^3m^{-3}) during 2016–2021 summer seasons from ERA5 at a grid cell (3.375°E, 48.478°N). The vertical red line marks the climatological threshold (SSM breakpoint; BP), while the red dot indicates the intersection of the two orange regressions lines (sampled separately from the dry and wet sides of the BP). The spatial distribution of (b) BP in SSM (units: m^3m^{-3}), (c) regression slope of TMAX on SSM on the dry side of BP, and (d) slope difference across the BP. The units in the maps relate to the slope: $K/(m^3m^{-3})$. (e–h) Bottom row of panels is the same as the upper row, but for GloSea5. (For interpretation of the references to colour in this figure legend, the reader is referred to the Web version of this article.)

days on the dry side of the BP, which quantifies the temperature response to the land surface dryness in the development of heatwave. For ERA5, the TMAX response in the dry soil moisture regions is stronger than in climatologically wet regions, which resembles the spatial pattern of the soil moisture climatology (Fig. 2c and d). For instance, over the Iberian Peninsula and the Northern European plain, the temperature increases by more than 10 K for a 0.1 m^3m^{-3} decrease in SSM. The spatial distribution of the dry side slope in GloSea5 does not agree well with ERA5 (Fig. 2g), where the pattern correlation between ERA5 and GloSea5 over Northern Europe (10°W–20°E, 45–65°N) is 0.67. GloSea5 exhibits stronger sensitivity in Southern Britain, Northern France, and Poland, and weaker sensitivity, which may contribute to underestimation of extreme high temperatures in the Northern European plain.

The slope difference between regression lines on the dry and wet side of the BP implies the nonlinearity of TMAX across the soil moisture state. The spatial distribution of the slope difference in ERA5 resembles the map of the slope on the dry side of the BP, since the temperature response to surface wetness is relatively insensitive to the slope on the wet side (Fig. 2d). The spatial agreement of the difference in slope for GloSea5 mirrors the dry side slope (Fig. 2h). The spatial correlation coefficient is 0.58 over the Northern Europe (10°W–20°E, 45–65°N), which indicates that GloSea5 has some fidelity to resolve the pattern of the nonlinear response of TMAX to soil water content. Notably, this spatial inconsistency of the regression slope on the dry side indicates that GloSea5 fails to simulate the strength of the hypersensitivity relative to the reanalysis, not that it cannot capturing the hypersensitivity.

To investigate the role of the hypersensitive regime in heatwave forecasts, this study assesses model performance with deterministic forecast skill metrics described in subsection 3.2. In the ERA5 reanalysis, when the soil water content is on the dry side of the BP, the skill metrics distinguish between whether the forecast model can capture the dry conditions or not: hits versus misses (Fig. S1). Heatwave prediction skill is evaluated by HR and TSS for each grid point (Fig. S2), depending on whether dry or wet soil moisture values are properly separated by the BP in the forecast model, and the heatwave prediction skill is composited for each lead time and ensemble member. Hit, false alarm, miss, or correct rejection, based on the contingency table for heatwave forecast validation, are composited by the model's ability to capture the hypersensitive regime (Fig. S3). The metrics are spatially averaged at various forecast leads. The HR metric indicates that there is skill improvement when GloSea5 correctly captures the reanalysis soil moisture relative to BP. Notably, at 5 days lead, when the hypersensitive regime is captured in the forecast model, the HR is 0.6, whereas misclassification leads to a significantly diminished predictive performance below 0.3 (Fig. 3a and S3). When extreme heat events occur, if the soil moisture condition is properly predicted in the dry regime, it can increase the heatwave skill score by more than 0.2 over 2-week lead forecast.

The TSS for hit cases exceeds that for misses by more than 0.23 in the 5-day lead forecast, consistently displaying superior performance in medium- and long-range forecasts. These results appear to be a notable increase of extreme forecast accuracy over 0.1 at 11 days lead when capturing the existence of the hypersensitive regime (Fig. 3b). Within the "hit" category, the intensity of TMAX exceeds that of the "miss" cases by more than 0.8 K; the disparity in lead times across 2 weeks accentuates this difference (Fig. 3c). Thus, a strong tendency towards higher temperatures during dry conditions contributes significantly to the prediction performance of extreme heat events. Correctly capturing the hypersensitive regime is a crucial resource for heatwave forecast skill. The role of land-atmosphere interactions in the prediction of heatwave events is important, and methods to accurately capture the correct soil moisture regime, e.g., through correct land initialization, can be considered important. Despite a fairly accurate simulation of the BP spatial distribution by the model, mediocre heatwave prediction performance by GloSea5 may be attributed to model fidelity in accurately simulating the slopes of the regression lines on both the dry and wet sides of the BP. Consequently, further quantitative evaluation of the

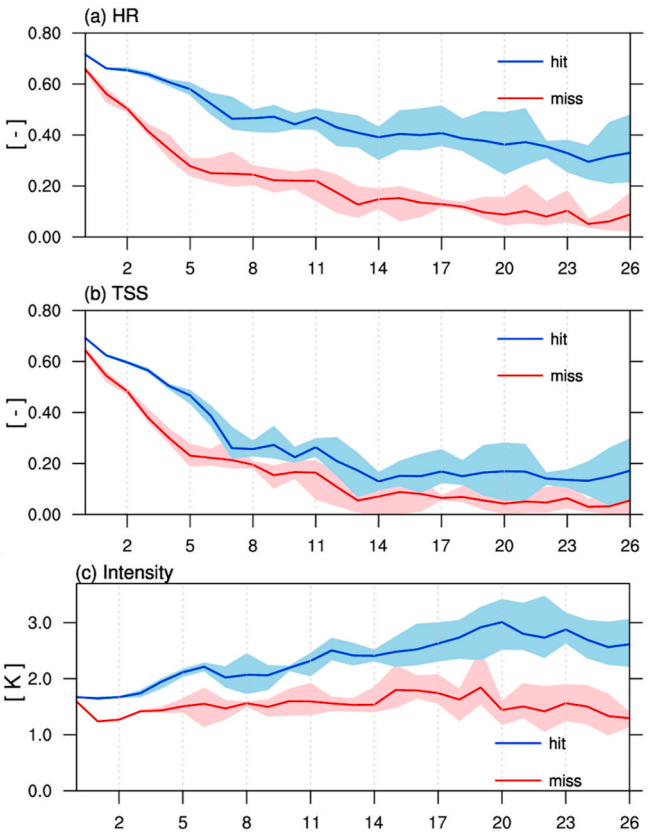

Fig. 3. Averaged skill scores for heatwaves prediction over Northern Europe (10°W–20°E, 45–65°N) across lead forecast time, for (a) HR, (b) TSS, and (c) Intensity, where blue and red lines are the results in which the model hit and miss SSM in the hypersensitive regime, respectively. Shading indicates upper and lower bounded values across 4 ensemble members. (For interpretation of the references to colour in this figure legend, the reader is referred to the Web version of this article.)

heatwave prediction performance with regard to model representation of temperature sensitivity to soil wetness is imperative.

Energy exchange at the land surface is controlled by the water and energy balance equations in the model. This study quantifies the strength of water-versus energy-limited processes by applying the temporal correlation coefficient to surface latent heat flux (Seo et al., 2024), which is a shared variable between both balance equations, as linked to SSM ($R(SSM,LE)$), and net radiation ($R(R_n,LE)$), respectively. To assess the fidelity of the land-atmosphere interactions in GloSea5, the spatial pattern of these two multivariate metrics is compared to ERA5. The land coupling regime in the reanalysis displays a meridional diploe structure over the Europe, which resembles the soil moisture climatology (Fig. 4a). The Iberian Peninsula has strong land-atmosphere coupling mostly explained by the water budget whereas energy-limited processes are weak because $R(R_n,LH)$ is close to zero (Fig. 4c and f). Although other regions exhibit stronger coupling with energy-limited process, there are some regions where the strength of water-versus energy-limited processes is comparable. The meridional dipole pattern is well captured by GloSea5 (Fig. 4b) with the dominance of the energy-limited processes located over the Northern Europe. However, there is a regional bias pattern. For instance, $R(R_n,LH)$ over the Iberian Peninsula is underestimated in the model and the Northern European region displays negative and positive biases in $R(SSM,LH)$ and $R(R_n,LH)$ respectively, corresponding to the kernel density estimation of the energy-limited coupling (Fig. 4e and h). The forecast model result corresponds to the widely spread distribution of the kernel density estimation of $R(SSM,LH)$, while there is a peak in ERA5 close to zero. The

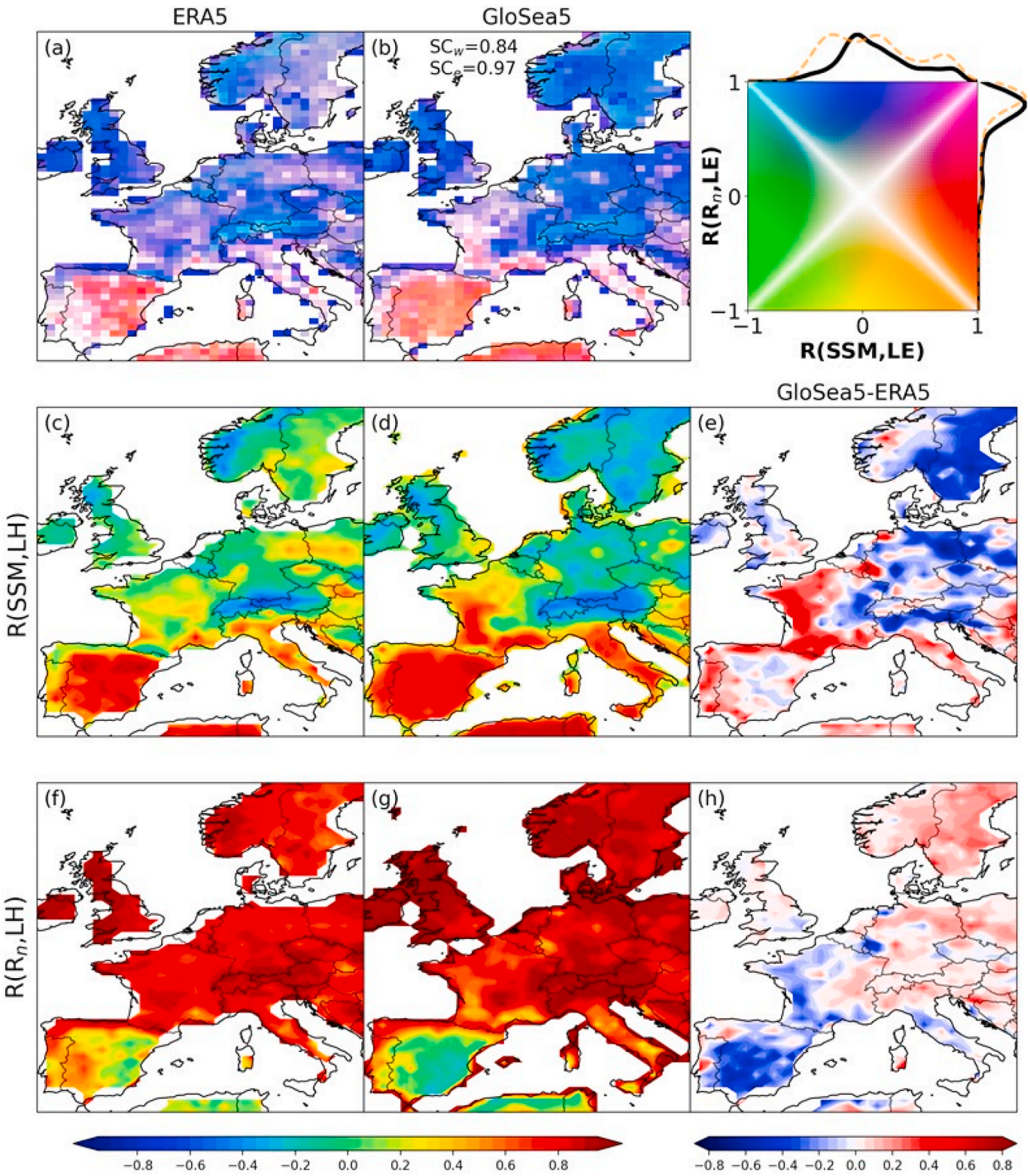

Fig. 4. Spatial distribution of land coupling regime metrics in (a) ERA5 and (b) GloSea5, where pattern correlations to characterize the spatial agreement of water- and energy-limited processes between GloSea5 and ERA5 are indicated with SC_w and SC_e, respectively. Shading indicates correlations as shown in the coloured square: LE and SSM (x-axis) and LE and net radiation R_n (y-axis). The distributions of the kernel density estimates from ERA5 (black) and GloSea5 (orange) along corresponding axes are also displayed. Each line is normalized by its maximum value. The spatial maps of $R(SSM, LE)$ (middle row) and $R(R_n, LE)$ (bottom row) are from ERA5 (leftmost column: c and f) and GloSea5 (middle column: d and g) over the European region. The bias maps of (e) water- and (h) energy-limited coupling are in the rightmost column. (For interpretation of the references to colour in this figure legend, the reader is referred to the Web version of this article.)

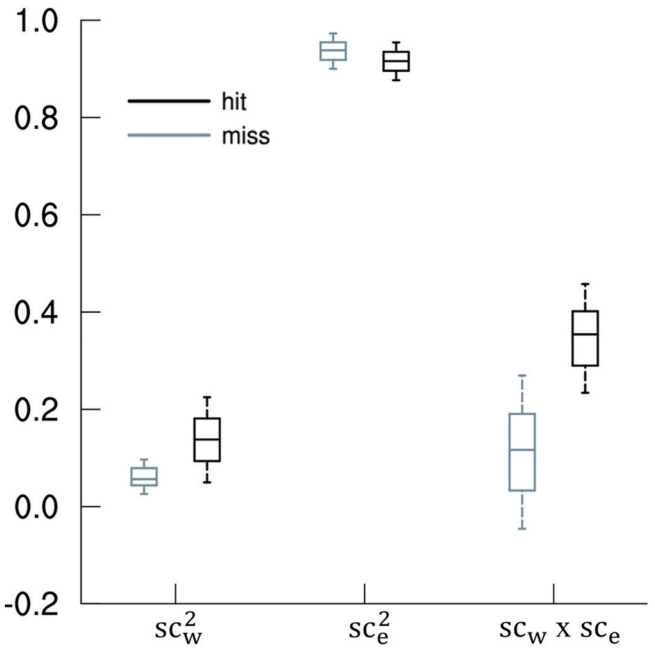

Fig. 5. Box plot of the squared spatial correlation coefficient as a measure of the spatial agreement of $R(SSM, LE)$ (SC_w) and $R(R_n, LE)$ (SC_e) when GloSea5 hits (black) and misses (gray) capturing SSM below BP compared to the ERA5 reanalysis over Northern Europe (10°W–20°E, 45–65°N). The comprehensive performance of the land coupling processes is quantified by $SC_w \times SC_e$ on the right. 248 samples (62 initialized runs having 4 ensemble members) are used to construct box plots where the box display the median and inter-quartile-range (IQR: 25th and 75th percentiles), and whiskers represent ±0.5 IQR from the 25th and 75th percentiles, respectively.

spatial correlation coefficients of $R(R_n, LH)$ (SC_e) and $R(SSM, LH)$ (SC_w) synthesize model performance. Energy-limited coupling is better represented than water-limited coupling: the spatial agreement of $R(R_n, LH)$ $(SC_e = 0.97)$ is higher than that of $R(SSM, LH)$ $(SC_w = 0.84)$ over Europe (10°W–20°E, 35–65°N). Previous studies have suggested that even in an energy-limited region, soil water content can still play an important role in land-atmosphere feedbacks, which means that soil moisture can be a potential factor in regulating the atmospheric behaviour (Koster et al., 2019), indicating that local climate can respond to land cover changes, climate changes, and agricultural practices (Chen and Dirmeyer 2020; Dirmeyer et al., 2013).

To synthesize model performance of the reproduction of observed land coupling, this study calculates SC_e and SC_w over Europe for each simulation and ensemble member (Fig. 5). In addition, to confirm the reproduction of observed land coupling according to the ability to capture the hypersensitive regime, this analysis is separately performed for the times and locations where the dry side of the BP is hit and missed. The model reproduces the observed energy-limited processes well with a squared spatial correlation (SC_e^2), and both hit (0.92) and miss (0.94) cases show comparable performance. On the other hand, in the case of the water-limited coupling, the model performs much worse: SC_w^2 is 0.14 and 0.05 for the hit and miss cases, respectively. The results imply that the performance of water-limited process is somewhat improved when the dry side is correctly represented. Formulating the combined squared spatial correlation $SC_w \times SC_e$ provides a comprehensive assessment of the land coupling in the model, offering insights into both water- and energy-limited processes. The representation of the land leg of coupling is enhanced when the BP is hit versus the missed case (Fig. 5), which primarily results in the increase of heatwave forecast skill (Fig. 3), accompanied with the comprehensive advance in the land coupling.

5. Summary and conclusions

This study has investigated the ability of the GloSea5 forecast model to predict the 2018 Northern Europe heatwave during the 2018 summer season and compares model performance corresponding to the effects of land-atmosphere interactions. Surface soil moisture (SSM) and maximum temperature (TMAX) have a negative relationship at the land surface since the partitioning of H among incoming net radiation increases with drying soil moisture. The sensitivity of TMAX to the SSM reveals a discontinuity in slope at a particular soil moisture value, a breakpoint (BP). Hypersensitivity in the soil moisture-temperature relationship appears on the dry side of the BP, in which the magnitude of the slope relating TMAX to SSM increases significantly. To understand the impact of the forecast model's ability to represent the BP on heatwave prediction skill, this study compares deterministic skill scores based on whether the model represents SSM in the hypersensitive regime. Thus, the potential sources contributing to land surface conditions exacerbating heatwaves are examined for heatwave prediction in the 2018 Northern Europe compound drought case.

The spatial distribution of BP simulated by GloSea5 resembles the ERA5 climatological pattern, displaying relatively high values in Northern Britain, Northern Scandinavia, and along the Alps, and dry values in much of the Northern European plain, southern Britain, and southern Scandinavia (Fig. 2b and f). However, in the model simulation, the regression slope between SSM and TMAX on the dry side of the BP and the slope difference between both sides show spatial disagreement with the observed pattern over Northern European plain and Portugal. This suggests that the model representation of soil moisture-temperature relationships could be improved in these areas. If the forecast system is able to simulate the dry side slope and the slope difference between both sides of the BP, the forecast skill would likely be further improved.

This study does not directly validate the climatological BP value in GloSea5 compared to ERA5 since there are physical inconsistencies between both products such as specified soil type, land cover type, and other land model parameters. When evaluating heatwave predictability in the model based on the fidelity of the land-atmosphere coupling, a contingency table is used for the classification of the SSM hit and miss relative to the BP of each. Heatwave cases are subsequently composited by the contingency table and deterministic forecast scores are calculated for each lead forecast time. When the model enters the hypersensitive regime, the observed TMAX is more reliably simulated by the realistic land-atmosphere coupling, which leads to increase skill scores. For the 5-day lead forecast, scores are more than twice as large when the forecast model correctly simulates SSM below the BP, and a heatwave intensity of 0.5 K higher is simulated (Fig. 2).

Land-atmosphere coupling is characterized as operating in either water- or energy-limited regimes based on SSM's position relative to a higher threshold, the critical soil moisture. Net radiation (energy availability) and soil wetness (water availability) regulated energy exchanges at the land surface on the wet and dry side of the critical SSM, respectively. The strength of both couplings is quantified by the temporal correlation coefficients of net radiation and SSM to latent heat. The meridional dipole pattern in ERA5 is accurately captured by GloSea5 (Fig. 4b). Nonetheless, a regional bias pattern arises because there are negative and positive biases of the energy-limited coupling in Northern Europe and the Iberian Peninsula (Fig. 4h), respectively, and an underestimation of water-limited coupling in the Northern European region (Fig. 4e). Spatial correlation synthesizes the model's ability to reproduce patterns of the water- and energy-limited processes.

Forecast model performance of the water- and energy-limited coupling is also compared depending on the ability to correctly predict whether a location is in the hypersensitive regime (Fig. 5). Although the impact of capturing the hypersensitive regime on the model fidelity of energy-limited processes is marginal, its effect in situations of water-limited coupling is compared with the missed cases. Therefore, the model's ability to simulate the hypersensitive regime in the soil

moisture-temperature relationship accounts for some of the heatwave forecast skill along with the presence of stronger land-atmosphere coupling, especially for water-limited situations.

This study illustrates the crucial role of soil moisture in heatwaves and underscores the importance of accurately capturing transitions of SSM into the hypersensitive regime in forecast models. It contributes to our understanding of land-atmosphere interactions in extreme weather events. The BP and the value of soil moisture relative to it are key predictors to simulate heatwaves in numerical models. Simulation of the value and patterns of BP, and evaluations of forecast capability to predict on which side of the BP soil moisture will be, helps us understand the effect of model fidelity on heatwave forecasts. This diagnosis provides insights into how accurately the model simulates the BP and quantitatively assesses the extent to which it can contribute to improving heatwave prediction. Additionally, this study highlights that although the regions of Europe where energy-limited coupling are pronounced, water-limited processes are also important to understanding the physical mechanisms of extreme heat events.

The GloSea5 forecast model does not incorporate realistic soil moisture initialization; accurate soil moisture initialization should also lead to enhancing forecast skill by correctly capturing the hypersensitive regime. Furthermore, this study does not indeed investigate the impact of the model fidelity representing the observed regression slope between the SSM and TMAX on the heatwave forecast. The dry side slope, which indicates the strength of the SM-TMAX coupling, should be taken into account to enhance the predictability of heat extremes. Therefore, forecast models demonstrate room for advancement because initial soil moisture conditions and the replication of the relationship between soil moisture and temperature extremes are not yet optimal. In the model development process, this insight may identify more precisely which parts need to be improved and which direction should be taken for model improvement.

CRediT authorship contribution statement

Sunlae Tak: Conceptualization, Investigation, Methodology, Software, Visualization, Writing – review & editing. **Eunkyo Seo:** Conceptualization, Investigation, Methodology, Software, Visualization, Writing – review & editing. **Paul A. Dirmeyer:** Conceptualization, Methodology, Writing – review & editing. **Myong-In Lee:** Conceptualization, Supervision, Writing – review & editing.

Declaration of competing interest

The authors declare that they have no known competing financial interests or personal relationships that could have appeared to influence the work reported in this paper.

Data availability

Data will be made available on request.

Acknowledgments

This work was funded by the Korea Meteorological Administration Research and Development Program under Grant KMI2017-02410 and the Pukyong National University Industry-university Cooperation Research Fund in 2023 (202311900001). ES was supported by the Korea Meteorological Administration Research and Development program under grant RS-2023-00241809. PAD's participation is via NOAA grant NA19NES4320002 to the Cooperative Institute for Satellite Earth System Studies (CISESS) via a subaward (79785-Z755420) to the Center for Ocean-Land-Atmosphere Studies at George Mason University.

Appendix A. Supplementary data

Supplementary data to this article can be found online at https://doi.org/10.1016/j.wace.2024.100670.

References

Barriopedro, D., García-Herrera, R., Ordóñez, C., Miralles, D.G., Salcedo-Sanz, S., 2023. Heat waves: physical understanding and scientific challenges. Rev. Geophys. 61.
Beck, H.E., Pan, M., Miralles, D.G., Reichle, R.H., Dorigo, W.A., Hahn, S., Sheffield, J., Karthikeyan, L., Balsamo, G., Parinussa, R.M., van Dijk, A.I.J.M., Du, J., Kimball, J. S., Vergopolan, N., Wood, E.F., 2021. Evaluation of 18 satellite- and model-based soil moisture products using in situ measurements from 826 sensors. Hydrol. Earth Syst. Sci. 25, 17–40.
Benson, D.O., Dirmeyer, P.A., 2021. Characterizing the relationship between temperature and soil moisture extremes and their role in the exacerbation of heat waves over the contiguous United States. J. Clim. 34, 2175–2187.
Benson, D.O., Dirmeyer, P.A., 2023. The soil moisture–surface flux relationship as a factor for extreme heat predictability in subseasonal to seasonal forecasts. J. Clim. 1–39.
Best, M.J., Pryor, M., Clark, D.B., Rooney, G.G., Essery, R.L.H., Menard, C.B., Edwards, J. M., Hendry, M.A., Porson, A., Gedney, N., Mercado, L.M., Sitch, S., Blyth, E., Boucher, O., Cox, P.M., Grimmond, C.S.B., Harding, R.J., 2011. The Joint UK land environment simulator (JULES), model description – Part 1: energy and water fluxes. Geosci. Model Dev. (GMD) 4, 677–699.
Bowler, N.E., Mylne, K.R., 2009. Ensemble transform Kalman filter perturbations for a regional ensemble prediction system. Q. J. R. Meteorol. Soc. 135, 757–766.
Chen, L., Dirmeyer, P.A., 2020. Reconciling the disagreement between observed and simulated temperature responses to deforestation. Nat. Commun. 11, 202.
Dirmeyer, P.A., 2006. The hydrologic feedback pathway for land–climate coupling. J. Hydrometeorol. 7 (5), 857–867.
Dirmeyer, P.A., Balsamo, G., Blyth, E.M., Morrison, R., Cooper, H.M., 2021a. Land-atmosphere interactions exacerbated the drought and heatwave over northern Europe during summer 2018. AGU Advances 2, e2020AV000283.
Dirmeyer, P.A., Balsamo, G., Blyth, E.M., Morrison, R., Cooper, H.M., 2021b. Land-atmosphere interactions exacerbated the drought and heatwave over northern Europe during summer 2018. AGU Advances 2, e2020AV000283.
Dirmeyer, P.A., Jin, Y., Singh, B., Yan, X., 2013. Evolving land–atmosphere interactions over north America from CMIP5 simulations. J. Clim. 26, 7313–7327.
Dirmeyer, P.A., Wu, J., Norton, H.E., Dorigo, W.A., Quiring, S.M., Ford, T.W., Santanello Jr., J.A., Bosilovich, M.G., Ek, M.B., Koster, R.D., Balsamo, G., Lawrence, D.M., 2016. Confronting weather and climate models with observational data from soil moisture networks over the United States. J. Hydrometeorol. 17, 1049–1067.
Findell, K.L., Gentine, P., Lintner, B.R., Kerr, C., 2011. Probability of afternoon precipitation in eastern United States and Mexico enhanced by high evaporation. Nat. Geosci. 4, 434–439.
Hamill, T.M., Juras, J., 2006. Measuring forecast skill: is it real skill or is it the varying climatology? Q. J. R. Meteorol. Soc. 132, 2905–2923.
Hersbach, H., Bell, B., Berrisford, P., Hirahara, S., Horányi, A., Muñoz-Sabater, J., Nicolas, J., Peubey, C., Radu, R., Schepers, D., Simmons, A., Soci, C., Abdalla, S., Abellan, X., Balsamo, G., Bechtold, P., Biavati, G., Bidlot, J., Bonavita, M., Chiara, G., Dahlgren, P., Dee, D., Diamantakis, M., Dragani, R., Flemming, J., Forbes, R., Fuentes, M., Geer, A., Haimberger, L., Healy, S., Hogan, R.J., Hólm, E., Janisková, M., Keeley, S., Laloyaux, P., Lopez, P., Lupu, C., Radnoti, G., Rosnay, P., Rozum, I., Vamborg, F., Villaume, S., Thépaut, J.N., 2020. The ERA5 global reanalysis. Q. J. R. Meteorol. Soc. 146, 1999–2049.
Hirschi, M., Seneviratne, S.I., Alexandrov, V., Boberg, F., Boroneant, C., Christensen, O. B., Formayer, H., Orlowsky, B., Stepanek, P., 2010. Observational evidence for soil-moisture impact on hot extremes in southeastern Europe. Nat. Geosci. 4, 17–21.
Kong, Q., Guerreiro, S.B., Blenkinsop, S., Li, X.-F., Fowler, H.J., 2020. Increases in summertime concurrent drought and heatwave in Eastern China. Weather Clim. Extrem. 28.
Koster, R.D., Schubert, S.D., Wang, H., Mahanama, S.P., DeAngelis, A.M., 2019. Flash drought as captured by reanalysis data: disentangling the contributions of precipitation deficit and excess evapotranspiration. J. Hydrometeorol. 20, 1241–1258.
Leach, N.J., Li, S., Sparrow, S., van Oldenborgh, G.J., Lott, F.C., Weisheimer, A., Allen, M.R., 2020. Anthropogenic influence on the 2018 summer warm spell in Europe: the impact of different spatio-temporal scales. Bull. Am. Meteorol. Soc. 101, S41–S46.
Loveland, T.R., Reed, B.C., Brown, J.F., Ohlen, D.O., Zhu, Z., Yang, L., Merchant, J.W., 2000. Development of a global land cover characteristics database and IGBP DISCover from 1 km AVHRR data. Int. J. Rem. Sens. 21, 1303–1330.
MacLachlan, C., Arribas, A., Peterson, K.A., Maidens, A., Fereday, D., Scaife, A.A., Gordon, M., Vellinga, M., Williams, A., Comer, R.E., Camp, J., Xavier, P., Madec, G., 2015. Global Seasonal forecast system version 5 (GloSea5): a high-resolution seasonal forecast system. Q. J. R. Meteorol. Soc. 141, 1072–1084.
Miralles, D., Van Den Berg, M., Teuling, A., De Jeu, R., 2012. Soil moisture-temperature coupling: a multiscale observational analysis. Geophys. Res. Lett. 39.
Miralles, D.G., Teuling, A.J., van Heerwaarden, C.C., Vilà-Guerau de Arellano, J., 2014. Mega-heatwave temperatures due to combined soil desiccation and atmospheric heat accumulation. Nat. Geosci. 7, 345–349.

Mogensen, K., Magdalena Alonso, B., Anthony, W., 2012. The NEMOVAR Ocean Data Assimilation System as Implemented in the ECMWF Ocean Analysis for System 4.
Pegion, K., Kirtman, B.P., Becker, E., Collins, D.C., LaJoie, E., Burgman, R., et al., 2019. The Subseasonal Experiment (SubX): a multimodel subseasonal prediction experiment. Bull. Am. Meteorol. Soc. 100 (10), 2043–2060.
Petch, J.C., Short, C.J., Best, M.J., McCarthy, M., Lewis, H.W., Vosper, S.B., Weeks, M., 2020. Sensitivity of the 2018 UK summer heatwave to local sea temperatures and soil moisture. Atmos. Sci. Lett. 21.
Quesada, B., Vautard, R., Yiou, P., Hirschi, M., Seneviratne, S.I., 2012. Asymmetric European summer heat predictability from wet and dry southern winters and springs. Nat. Clim. Change 2, 736–741.
Rae, J.G.L., Hewitt, H.T., Keen, A.B., Ridley, J.K., West, A.E., Harris, C.M., Hunke, E.C., Walters, D.N., 2015. Development of the global sea ice 6.0 CICE configuration for the Met Office global coupled model. Geosci. Model Dev. (GMD) 8, 2221–2230.
Santanello, J.A., Dirmeyer, P.A., Ferguson, C.R., Findell, K.L., Tawfik, A.B., Berg, A., Ek, M., Gentine, P., Guillod, B.P., van Heerwaarden, C., Roundy, J., Wulfmeyer, V., 2018. Land–atmosphere interactions: the LoCo perspective. Bull. Am. Meteorol. Soc. 99, 1253–1272.
Seneviratne, S.I., Corti, T., Davin, E.L., Hirschi, M., Jaeger, E.B., Lehner, I., Orlowsky, B., Teuling, A.J., 2010. Investigating soil moisture–climate interactions in a changing climate: a review. Earth Sci. Rev. 99, 125–161.
Seo, E., Dirmeyer, P.A., Barlage, M., Wei, H., Ek, M., 2024. Evaluation of land-atmosphere coupling processes and climatological bias in the UFS global coupled model. J. Hydrometeorol. 25 (1), 161–175.
Seo, E., Dirmeyer, P.A., 2022a. Improving the ESA CCI daily soil moisture time series with physically-based land surface model datasets using a Fourier time-filtering method. J. Hydrometeorol.
Seo, E., Dirmeyer, P.A., 2022b. Understanding the diurnal cycle of land–atmosphere interactions from flux site observations. Hydrol. Earth Syst. Sci. 26, 5411–5429.
Seo, E., Lee, M.-I., Jeong, J.-H., Koster, R.D., Schubert, S.D., Kim, H.-M., Kim, D., Kang, H.-S., Kim, H.-K., MacLachlan, C., Scaife, A.A., 2019. Impact of soil moisture initialization on boreal summer subseasonal forecasts: mid-latitude surface air temperature and heat wave events. Clim. Dynam. 52, 1695–1709.
Seo, E., Lee, M.-I., Schubert, S.D., Koster, R.D., Kang, H.-S., 2020. Investigation of the 2016 Eurasia heat wave as an event of the recent warming. Environ. Res. Lett. 15.
Suarez, M.J., Koster, R.D., Wang, H., Schubert, S.D., Groisman, P.Y., 2014. Northern eurasian heat waves and droughts. J. Clim. 27, 3169–3207.
Tartaglione, N., 2010. Relationship between precipitation forecast errors and skill scores of dichotomous forecasts. Weather Forecast. 25, 355–365.
Walters, D., Boutle, I., Brooks, M., Melvin, T., Stratton, R., Vosper, S., Wells, H., Williams, K., Wood, N., Allen, T., Bushell, A., Copsey, D., Earnshaw, P., Edwards, J., Gross, M., Hardiman, S., Harris, C., Heming, J., Klingaman, N., Levine, R., Manners, J., Martin, G., Milton, S., Mittermaier, M., Morcrette, C., Riddick, T., Roberts, M., Sanchez, C., Selwood, P., Stirling, A., Smith, C., Suri, D., Tennant, W., Vidale, P.L., Wilkinson, J., Willett, M., Woolnough, S., Xavier, P., 2017. The Met Office unified model global atmosphere 6.0/6.1 and JULES global land 6.0/6.1 configurations. Geosci. Model Dev. (GMD) 10, 1487–1520.
Wehrli, K., Hauser, M., Seneviratne, S.I., 2020. Storylines of the 2018 Northern Hemisphere heatwave at pre-industrial and higher global warming levels. Earth System Dynamics 11, 855–873.